Magnetized Bentonite Clay Particles for Lithium adsorption

Mojalefa W Modiba and Elvis Fosso-Kankeu

***Abstract*— Bentonite is a porous clay material known for its effective adsorption of heavy metals. In this study, we developed magnetic bentonite by incorporating Fe_3O_4 particles onto aluminum-pillared bentonite (Al-Bentonite) to enhance its removal from water. We analyzed the functional groups and elemental composition of the modified material using FT-IR and XRF techniques. The magnetic bentonite was then tested as an adsorbent for lithium removal from aqueous solutions, and we examined how various parameters affected its adsorption performance. Different kinetic models were applied to identify the best fit for the experimental data, with the pseudo-second-order model providing the best fit for both raw and activated samples. The thermodynamic parameter ΔH was calculated as 2.202 kJ/mol for raw bentonite and 3.437 kJ/mol for activated bentonite, indicating a chemical adsorption process.**

Overall, the thermodynamic analysis suggested that lithium adsorption is endothermic and non-spontaneous. The negative entropy values (ΔS) of -5.9663 J/mol·K for raw and -2.446 J/mol·K for activated bentonite indicate potential structural changes or adjustments in the adsorbate-adsorbent complex during adsorption. Additionally, lithium adsorption efficiency increased with temperature, achieving a maximum of 23.75% for the raw sample and 18.82% for the activated sample at 55 °C.

***Keywords*— Magnetized bentonite clay particles, vanadium, adsorption.**

I. Introduction

Rapid industrial growth has led to an increase in heavy metals being released in mining effluents. To recover lithium from these effluents, several methods have been developed, including chemical precipitation, electrolytic reduction, membrane filtration, reverse osmosis, adsorption, and ion exchange [1]. Among these, adsorption is particularly effective due to its efficiency, ease of use, and cost-effectiveness. Adsorption is one of the best recovery techniques because of its low cost, easy to use and high efficiency to recover base metals. The adsorption capacity of adsorbent can be determined by use of adsorption isotherm [2]. Various adsorbents, particularly activated carbon, have been carefully studied, providing effective results [3-10].

However, it is not the best option for industrial applications due to difficulties with its high cost and separation procedures [11]. Bentonite is one of the best adsorbent materials owing to its excellent adsorption capacity, natural availability, chemical and physical stability, outstanding cation exchange capacity when mixed with water, low-cost and high surface area enabling it to adsorb base metals [12]. Various modification techniques were developed by inserting functional groups and mineral composite to bentonite, to convert soluble or available base metal ions into insoluble states, and then to improve the long-term base metal retention capacity of bentonite.

Iron oxide has been found to be the best reliable magnetizing agent since it has magnetic properties, the ability to be recycled and can be separated from the solutions more readily [11]. The bentonite clay mineral supported magnetite nanoparticles prepared by co-precipitation [13]. According to Mockovčiaková et al. [14], the findings indicate that in cases when the starting concentration of the metals under study is very low, magnetic bentonite is a better sorbent than unmodified bentonite.

The aim of this study is to develop a cost-effective and efficient method for lithium adsorption using magnetized bentonite clay particles.

II. METHODOLOGY

A. Preparation of the adsorbent (γ-Fe2O3@Mt)

The γ-Fe_2O_3@Mt was prepared using co-precipitation method of Fe^{2+} and Fe^{3+} in alkaline solution in the presence of raw Mt. The typical synthesis process is as follows: At first, weigh the correct mass of Mt (50 g) and disperse it in 900 ml of deionized water in ultrasonic bath. Then, 100 ml of a solution containing 1 M of $FeCl_2.4H_2O$ and 2M of $FeCl_3$ at a ratio of 1:2 was prepared and added to the prepared Mt suspension. Finally, the basic solution of NH_4OH (2M) was added dropwise under stirring at 60°C temperature for 4 h. The resulting product was washed with deionized water to remove unbound magnetite nanoparticles and to control the pH of the adsorbent. The initial pH of 2.47 was brought 6.88 by washing the adsorbent for 12 days and dried at a temperature of 150 °C for 3 days.

B. Characterization of Magnetized Bentonite Clay Particles

Used Fourier transform infrared (FTIR) spectroscopy technique and X-ray fluorescence (XRF) to analyse the structure and morphology of the magnetized bentonite clay particles.

C. Adsorption experimental procedure

The lithium adsorption experiments was done in different

Mojalefa W Modiba, Department of Metallurgy at the University of Johannesburg in South Africa.

Elvis Fosso-Kankeu, Department of Metallurgy at the University of Johannesburg in South Africa.

time ranges (20,40,60,80, and 100 min), and different temperature (25, 35, 45, and 55℃). The solution containing lithium was prepared by mixing lithium carbonate(Li_2CO_3) of mass with deionized water on a magnetic stirrer in a beaker. The dissolution of the salt was aided by adding solid sodium hydroxide(NaOH) at a high rotational speed (600rpm) and thereafter the solution was poured in a volumetric and filled to the mark using deionized water to achieve a stock solution a 1000ppm. The pH of the metal solution was measured to be 4,05 using a pH meter, mass of adsorbent was kept at 0.14g, the volume of the solution was 100 mL in each conical flask using the experiment. The magnetized clay mineral γ-Fe_2O_3@Mt was tested for removal of the lithiium from aqueous solutions using the batch adsorption technique. The adsorption tests will be carried out using a series of conical flasks (250 ml) containing 100 ml of Li_2CO_3 at a fixed initial concentration of 50 ppm. Then, the 0.14g of γ-Fe_2O_3@Mt was added in each flask and the solutions was agitated at a constant speed of 200 rpm.

The batch adsorption experiment was done at room temperature (25℃) for 20, 40, 60, 80, and 100 minutes. The same was repeated at a temperature of 35, 45, and 55℃. After each experiment, the adsorbent was separated from the aqueous solution using filtration, and an atomic absorption spectrometer (AAS) was used to measure the concentration of vanadium in the samples. For adsorption kinetics, the effect of contact time (20–100 min) will be evaluated. Then the percentage removal of vanadium by the magnetized bentonite clay particles calculated.

III. Results And Discussion

A. Characterisation of the Adsorbent

After the adsorbent have been prepared like mention in the methodology, both the raw bentonite clay and activated bentonite clay from magnetizing synthesis were submitted for XRF, FTIR, and SEM analysis to characterize them and observe the changes. Below in table I are a summary of XRF analysis results showing where there were significant changes to be studied. As XRF revels the elemental composition of the raw bentonite clay and activated bentonite clay, the following elements have shown a declined in the weight percentage (%wt): Na, Mg, Al, Si, K, and Ca. But more importantly the Fe weight percentage (%wt) has increased from 5.9132 %wt to 19.717 %wt as seen in the table. Meaning the activation of the sample could have worked since the iron oxide content has increased significantly than any other oxide or element.

TABLE I: XRF RESULTS THE ELEMENTAL COMPOSITION OF THE SAMPLES

Sample A (Raw Bentonite Clay)				Sample B (Activated Bentonite Clay)			
Oxides %w		Corrected %w		Oxides %w		Corrected %w	
Na2O	1,3803	Na	1,0240	Na2O	0,2198	Na	0,1631
MgO	3,2363	Mg	1,9517	MgO	2,2770	Mg	1,3732
Al2O3	15,988	Al	8,4613	Al2O3	13,925	Al	7,3696
SiO2	66,575	Si	31,122	SiO2	53,173	Si	24,856
K2O	1,3175	K	1,0937	K2O	0,7915	K	0,6571
CaO	1,9954	Ca	1,4261	CaO	0,3648	Ca	0,2607
Fe2O3	8,4541	Fe	5,9132	Fe2O3	28,190	Fe	19,717

Again the samples were characterized using FTIR for structural characterisation as It helps identify structural features such as O-H groups, Al-O, and Si-O bonds. It also allows to examine structural modifications in clay minerals upon chemical treatments, such as acid activation. Below in Figure 2 represents the raw bentonite clay, here five peaks orientation at: 3436.21 cm-1(8.21%T), 1637.13 cm-1(36.68%T), 1384.16 cm-1(29.03%T), 1037.61 cm-1(1.40%T), and 795.56 cm-1(62.29%T). These five were found to have these functional groups: O-H, H-O-H, O-H, Si-O, and Al-O-Si repectively.

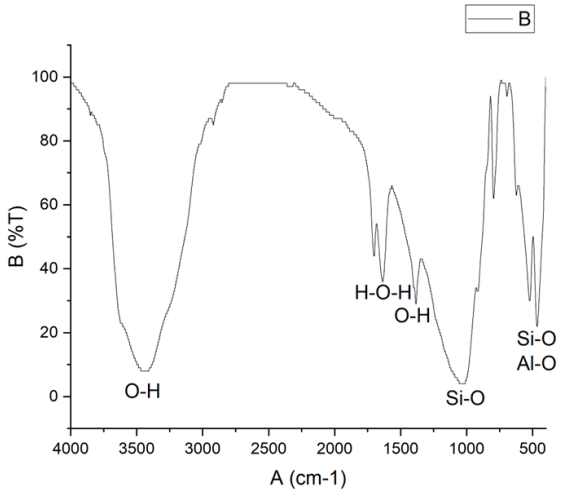

Fig. 1: Graph showing FTIR analysis of the raw sample

And their vibration bands were determined in Table II below showing their strengths. The first and fourth peaks in the table below suggests a significant absorption with their vibration bands of strong-stretching while others show a moderate absorption.

TABLE II: A TABLE SHOWING VIBRATIONS OF THE PEAKS OF THE RAW SAMPLE

Raw Bentonite Clay			
Wavenumber (cm-1)	%T	Functional group	Vibrations
3436,21	8,21	O-H	Strong-stretching
1637,13	36,7	H-O-H	Bending
1384,16	29,1	O-H	Deformation
1037,61	1,40	Si-O	Strong-stretching
795,56	62,3	Al-O-Si	Bending

Below in Figure 3 represents the activated bentonite clay, here five peaks orientation at: 3435.73cm-1(14.84%T), 1634.68 cm-1(86.76%T), 1385.22 cm-1(59.63%T), 1045.61 cm-1(1.40%T), and 523.81 cm-1(1.34%T). These five were found to have these functional groups: O-H, H-O-H or O-H, -OH, Si-O, and Al-O & Si-O repectively. There are slightly changes when considering the wavelength except for the last wavelength in Table II and III when coamparing the FTIR analysis of the raw and activated bentonite clay. But there is a significant variation when comaparing their transimittance value (%T) and vibration bands of each wavelength. These variations represents the structural modifications in clay minerals samples submitted upon chemical treatments during when the sample was being magnetized using iron oxide.

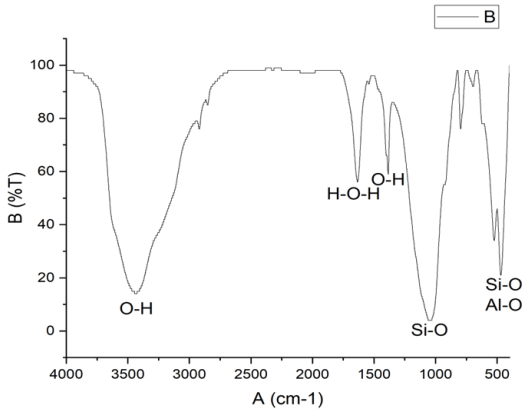

Fig. 2: Graph showing FTIR analysis of the activated sample

And their vibration bands were determined in Table III below showing their strengths. The first and second peaks in the table below suggests a significant absorption with their vibration bands of strong-stretching and strong-bending respectively, while others show a moderate absorption. Their structural modifications in clay minerals samples will results in different adsorption efficiencies and adsorption kinetics.

TABLE III: A TABLE SHOWING VIBRATIONS OF THE PEAKS OF THE ACTIVATED SAMPLE

Activated Bentonite Clay			
Wavenumber (cm-1)	%T	Functional group	Vibrations
3435,73	14,8	O-H	Strong-stretching
1634,68	86,8	O-H or H-O-H	Strong-bending
1385,22	59,7	O-H	Bending
1045,61	1,40	Si-O	Stretching
523,81	1,34	Si-O : Al-O	Bending

B. Adsorption results

Figure 4 below shows the graph comparing lithium adsorption efficiency of raw and activated bentonite clay at 25°C and 35°C over 20 to 100 minutes. Raw bentonite at 25°C achieved the highest recovery of about 20%, indicating optimal adsorption at room temperature. At 35°C, it started with a lower recovery of around 10% but improved to approximately 17% by the end. Activated bentonite showed consistent recoveries around 17% at both temperatures, suggesting that activation stabilizes performance without significantly enhancing capacity. Most lithium uptake occurred within the first 40 minutes, approaching equilibrium afterward, particularly in raw bentonite at 35°C. Overall, while activated bentonite provides reliable results, raw bentonite at room temperature may be more cost-effective for lithium recovery, though the low recovery rates (10-20%) suggest room for improvement in the process.

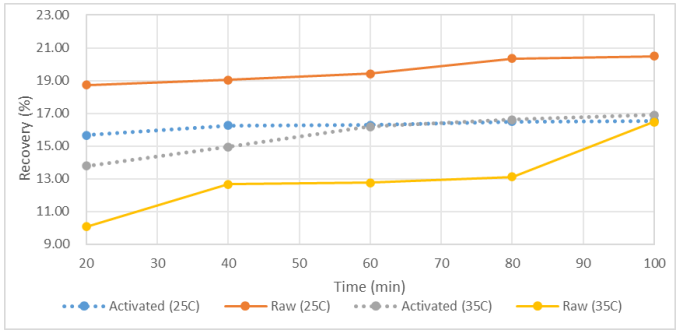

Fig. 3: A graph showing recoveries of both samples at 25 and 35 C temperatures

The graph in Figure 5 depicts lithium adsorption behavior of raw and activated bentonite clay at higher temperatures (45°C and 55°C) over 20 to 100 minutes. Raw bentonite at 55°C showed the most significant improvement, starting at about 14.5% recovery and reaching approximately 23.5% by the end. Raw bentonite at 45°C also improved, achieving around 22% recovery. In contrast, activated bentonite demonstrated modest gains, with the 55°C sample increasing from 17% to 19%, and the 45°C sample rising slightly from 16% to 17%. These results suggest that higher temperatures enhance raw bentonite's adsorption capacity due to increased molecular mobility, while activation limits temperature benefits. The ongoing increase in recovery for raw samples, particularly at 55°C, indicates potential for even higher recovery rates with extended contact time, making this temperature range likely optimal for lithium recovery from Li_2CO_3 solutions using raw bentonite.

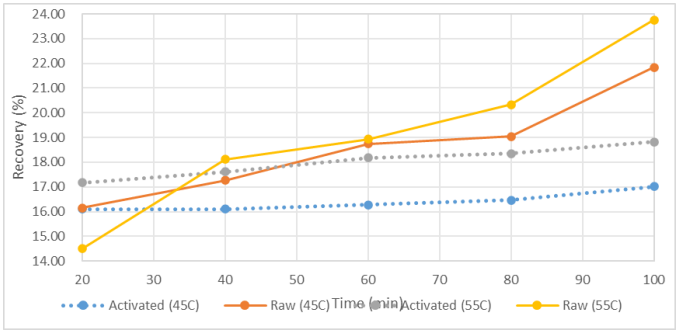

Fig. 4: A graph showing recoveries of both samples at 45 and 55 C temperatures

C. Adsorption Kinetics

Figure 6 and 7 looked at how lithium is adsorbed onto raw clay at four different temperatures (25°C, 35°C, 45°C, and 55°C) using two models: pseudo-first-order and pseudo-

second-order. The pseudo-first-order model showed that the rate of adsorption was fastest at 25°C, where the slope was steepest. In contrast, the pseudo-second-order model provided clearer and more consistent results across all temperatures, with the strongest increase seen at 35°C. This suggests that the adsorption process mainly follows the pseudo-second-order model, indicating that chemical bonding might be the slowest step in the process. Additionally, at higher temperatures (45°C and 55°C), the lines in this model were close together, suggesting similar adsorption behaviors.

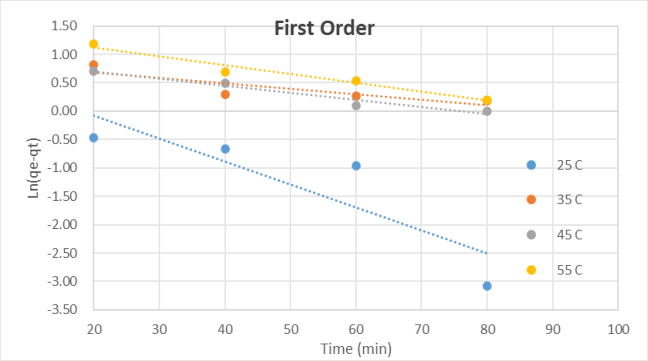

Fig. 5: A graph of first order kinetics of the raw sample

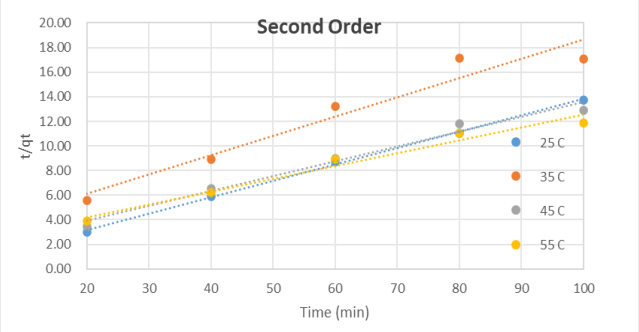

Fig. 6: A graph of second order kinetics of the raw sample

In Figure 8 and 9 the graphs illustrate kinetic modeling data for lithium adsorption onto activated bentonite clay at temperatures of 25°C, 35°C, 45°C, and 55°C. The first graph focuses on pseudo-first-order kinetics, plotting Ln(qe-qt) against time, while the second graph examines pseudo-second-order kinetics through the t/qt versus time relationship. The results indicate that the pseudo-second-order model offers a superior fit for the adsorption process, as evidenced by more linear relationships and higher correlation coefficients across all temperatures. This suggests that lithium adsorption likely follows pseudo-second-order kinetics, with chemisorption potentially serving as the rate-limiting step. Furthermore, both graphs reveal that temperature significantly influences the adsorption process; higher temperatures correlate with increased adsorption rates. This is particularly noticeable in the pseudo-second-order plot, where varying slopes indicate that both adsorption capacity and rate constants are influenced by temperature changes.

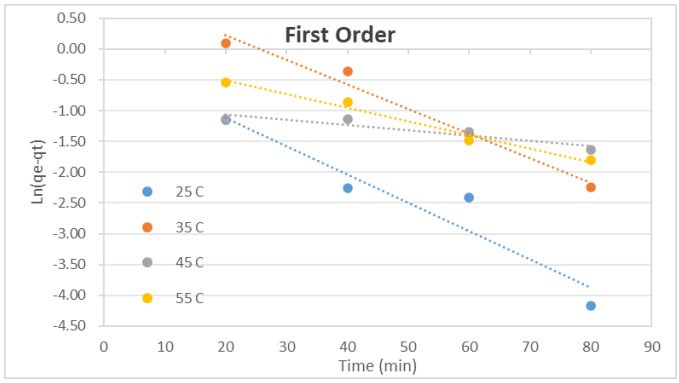

Fig. 7: A graph of first order kinetics of the activated sample

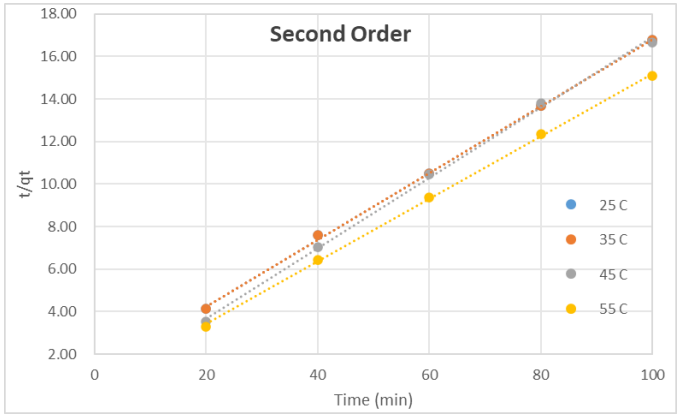

Fig. 8: A graph of second order kinetics of the activated sample

A comparison of lithium adsorption between raw and activated bentonite clay from Table X and XI in the appendix reveals that activated clay significantly outperforms raw clay. Activated clay shows higher R^2 values for both pseudo-first-order (mean R^2 = 0.93375) and pseudo-second-order (mean R^2 = 0.995025) kinetics, compared to raw clay's values of 0.8591 and 0.913825, indicating improved predictability and consistency in adsorption. The rate constants for both clays are temperature-dependent, but activated clay exhibits more uniform behavior. The pseudo-second-order model fits both types well, with a more pronounced improvement in activated clay, suggesting enhanced chemical adsorption. Additionally, activated clay has a higher potential adsorption capacity (1/qe mean = 0.158325) than raw clay (mean = 0.134175), indicating that activation creates a more efficient surface for lithium removal.

D.Adsorption Thermodynamics

The graph in Figure 10 displays adsorption thermodynamics by plotting Ln(k) against 1000/T(K-1) for contact times of 20 to 100 minutes using a raw clay sample. The negative Ln(k) values (from -1.0 to -2.2) suggest that higher temperatures make the adsorption process less favorable, indicating it is exothermic. Each line for different contact times shows a downward trend with increasing temperature, typical of physical adsorption where adsorbate-adsorbent interactions weaken. While there are variations in equilibrium conditions based on contact duration, the overall

thermodynamic behavior remains consistent across the different times.

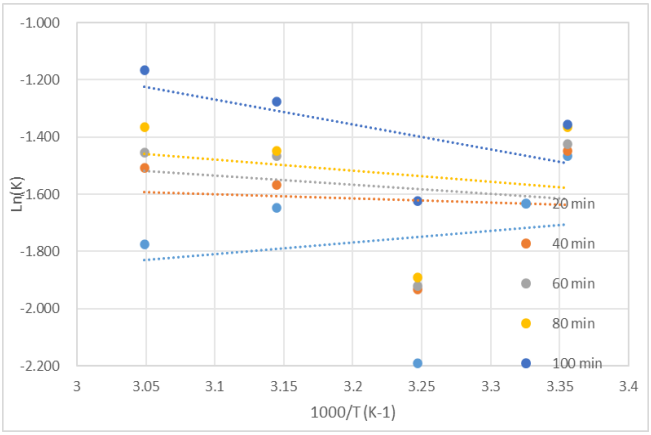

Fig. 9: A graph presenting of thermodynamics data of the raw clay sample

The thermodynamic analysis of the raw clay sample shows distinct trends across contact times of 20 to 100 minutes as observed in Table IV. Correlation coefficients (R^2) vary from low (0.0077 at 40 minutes) to moderate (0.3495 at 100 minutes), indicating inconsistent data fitting. The enthalpy change (ΔH) shifts from endothermic at -3.383 kJ/mol at 20 minutes to exothermic at 7.268 kJ/mol at 100 minutes. The entropy change (ΔS) becomes less negative with longer contact times, increasing from -25.537 to 11.981 J/mol·K, which suggests greater disorder in the system. Gibbs free energy (ΔG) decreases from 7606.7 to -3563.2 kJ/mol, with the negative value at 100 minutes indicating that the adsorption process becomes spontaneous over time. Overall, these findings suggest that adsorption on raw clay becomes more favorable and spontaneous with increased contact time due to enhanced interactions between the adsorbate and the clay surface.

TABLE IV: A TABLE OF THERMODYNAMICS DATA OF THE RAW CLAY SAMPLE

Raw Clay				
Time (min)	**R^2**	**ΔH**	**ΔS**	**ΔG**
20	0,0306	-3,383	-25,537	7606,7
40	0,0077	1,201	-9,574	2854,4
60	0,0320	2,671	-4,479	1337,3
80	0,0419	3,253	-2,207	661,0
100	0,3495	7,268	11,981	-3563,2
mean	0,0923	2,202	-5,963	1779,3

The graph in Figure 11 presents the adsorption thermodynamics for activated clay, which shows more consistent and uniform behavior than raw clay. The Ln(k) values range from approximately -1.4 to -1.9, indicating a narrower distribution. All contact times (20-100 minutes) exhibit parallel negative slopes, reflecting a consistent exothermic adsorption process. The closer spacing of the lines suggests that the activation process has resulted in a more homogeneous surface for adsorption. This improved uniformity leads to more predictable and efficient adsorption behavior. Overall, the narrower range of Ln(k) values indicates that activated clay reaches equilibrium more reliably across different temperatures and contact times, showcasing enhanced adsorption performance compared to the raw clay sample.

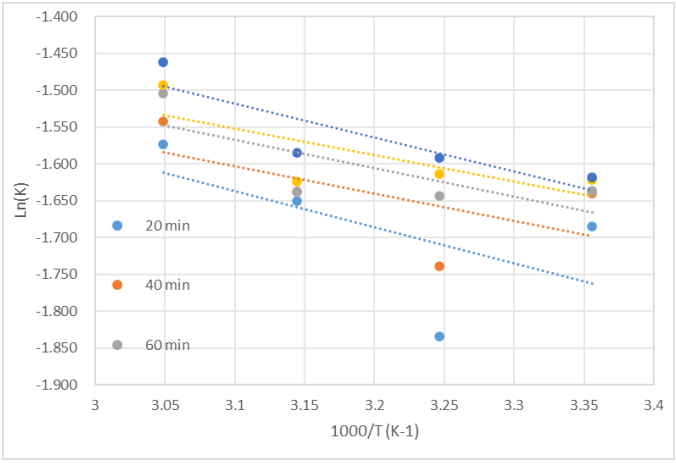

Fig. 10: A graph presenting of thermodynamics data of the activated clay sample

The thermodynamic parameters for the activated clay sample show significant improvements over the raw clay, with R^2 values ranging from 0.3515 to 0.7571, indicating better correlation and reliable data fitting, especially at longer contact times as observed in Table V. The positive ΔH values (2.985 to 4.076 kJ/mol, mean of 3.437 kJ/mol) suggest an endothermic adsorption process consistent across all contact durations. Negative ΔS values (from -0.785 to -3.730 J/mol·K, mean of -2.446 J/mol·K) indicate decreased disorder at the solid-solution interface during adsorption. While the positive ΔG values (237.7 to 1114.8 kJ/mol, mean of 732.3 kJ/mol) show the process is non-spontaneous, the lower ΔG values compared to raw clay suggest that activation enhances the adsorption process's energetic favorability. Overall, these consistent parameters and higher R^2 values indicate that activation has created a more uniform surface with homogeneous adsorption sites, leading to more efficient and predictable adsorption behavior.

TABLE V: A TABLE OF THERMODYNAMICS DATA OF THE RAW CLAY SAMPLE

Activated Clay				
Time (min)	**R^2**	**ΔH**	**ΔS**	**ΔG**
20	0,3515	4,076	-0,973	294,0
40	0,3748	3,095	-3,730	1114,8
60	0,5668	3,208	-3,087	923,1
80	0,5549	2,985	-3,654	1091,9
100	0,7571	3,819	-0,785	237,7
mean	0,5210	3,437	-2,446	732,3

IV. Conclusion

When comparing pseudo-first and second-order models at temperatures ranging from 25°C to 55°C, the pseudo-second-order kinetics demonstrates superior fit with highly linear relationships and better correlation coefficients just as mention in the literature review. This suggests that chemisorption,

involving chemical bonding between lithium ions and the clay surface, is the primary rate-limiting step in the adsorption process. Activated clay shows higher R^2 values for both pseudo-first-order (mean R^2 = 0.93375) and pseudo-second-order (mean R^2 = 0.995025) kinetics, compared to raw clay's values of 0.8591 and 0.913825, indicating improved predictability and consistency in adsorption.

The temperature dependence is clearly evident, with higher temperatures (55°C) showing enhanced adsorption rates 23.75 and 18.82% for raw and activated clay samples respectively compared to lower temperatures (25°C), indicated by the varying slopes in the pseudo-second-order plot. The recoveries of these adsorbent are very low when compared to the one in literature review by Hoyer et al., (2015) because Li in water has a thick layer of water molecules around it, it struggles to get close to the mineral surfaces and mainly forms outer sphere complexes. Therefore, many exchange sites in bentonite remain unused by Li. And thus the aim is not achieved since the activation of the samples stabilizes the adsorption efficiency instead of improving it but the objectives were achived as presented in the results.

The thermodynamics of the activated clay indicated an R^2 of with the reaction being endothermic due to mean ΔH = 3.437 kJ/mol being positive. The negative entropy of mean ΔS = -2.446 J/mol·K represents the randomness of the adsorbent which occurred during modifying it. While the positive ΔG values (mean of 732.3 kJ/mol) show the process is non-spontaneous, the lower ΔG values compared to raw clay suggest that activation enhances the adsorption process's energetic favorability. Overall, these consistent parameters and higher R^2 values indicate that activation has created a more uniform surface with homogeneous adsorption sites, leading to more efficient and predictable adsorption behavior. Correlation coefficients (R^2) vary from low 0.0077 to moderate 0.3495 as time increases, indicating inconsistent data fitting of the raw clay. The enthalpy change (ΔH) shifts from endothermic at -3.383 kJ/mol at 20 minutes to exothermic at 7.268 kJ/mol at 100 minutes.

ACKNOWLEDGMENT

The authors are grateful for the financial support received from the Faculty of Engineering and the Built Environment at the University of Johannesburg.

REFERENCES

[1] Zou, C., Liang, J., Jiang, W., Guan, Y. and Zhang, Y., 2018. Adsorption behavior of magnetic bentonite for removing Hg (II) from aqueous solutions. RSC advances, 8(48), pp.27587-27595. https://doi.org/10.1039/C8RA05247F

[2] Iakovleva, E. and Sillanpää, M., 2013. The use of low-cost adsorbents for wastewater purification in mining industries. Environmental Science and Pollution Research, 20, pp.7878-7899. https://doi.org/10.1007/s11356-013-1546-8

[3] Nthambeleni Mukwevho, Elvis Fosso-Kankeu, Frans Waanders, Neeraj Kumar, Suprakas Sinha Ray, Xavier Yangkou Mbianda. 2019. Evaluation of the photocatalytic activity of Gd2O2CO3.ZnO.CuO nanocomposite used for the degradation of phenanthrene. Springer Nature Applied Sciences. https://doi.org/10.1007/s42452-018-0012-0. 1-10.

[4] Elvis Fosso-Kankeu, Frans B. Waanders, Frederik W. Steyn. 2017. Removal of Cr(VI) and Zn(II) from an aqueous solution using an organic-inorganic composite of bentonite-biochar-hematite. Desalination and Water Treatment. 59: 144-153. https://doi.org/10.5004/dwt.2016.0059

[5] E. Fosso-Kankeu, F. Waanders, E. Maloy. 2016. Copolymerization of ethyl acrylate onto guar gum for the adsorption of Mg (II) and Ca (II) ions. Desalination and Water Treatment. doi: 10.1080/19443994.2016.1165147: 1-10. https://doi.org/10.1080/19443994.2016.1165147

[6] Elvis Fosso-Kankeu, Frans. B. Waanders, Frederik W. Steyn. 2015. The Preparation and Characterization of Clay-Biochar Composites for the Removal of Metal Pollutants. 7thInternational Conference on Latest Trends in Engineering and Technology (ICLTET' 2015), November 26-27, 2015 Irene, Pretoria (South Africa). Editors: E. Muzenda and T Yingthawornsuk. ISBN: 978-93-84422-58-5.

[7] A. Manyatshe, E. Fosso-Kankeu, D. van der Berg, N. Lemmer, F. Waanders, H. Tutu. 2017. Dispersion of inorganic contaminants in surface water in the vicinity of Potchefstroom. Physics and Chemistry of the Earth. 100: 86-93. https://doi.org/10.1016/j.pce.2017.04.008

[8] E Fosso-Kankeu. 2018. Synthesized af-PFCl and GG-g-P(AN)/TEOS hydrogel composite used in hybridized technique applied for AMD treatment. Journal of Physics and Chemistry of the Earth. 105: 170-176. https://doi.org/10.1016/j.pce.2018.02.015

[9] E. Fosso-Kankeu, A.F. Mulaba-Bafubiandi, L.A. Piater, M.G. Tlou. 2016. Cloning of the cnr operon into a strain of Bacillaceae bacterium for the development of a suitable biosorbent. World Journal of Microbiology and Biotechnology. DOI 10.1007/s11274-016-2069-5. https://doi.org/10.1007/s11274-016-2069-5

[10] E. Fosso-Kankeu, A.F. Mulaba-Bafubiandi, T.G. Barnard. 2014. Establishing suitable conditions for metals recovery from metal saturated Bacillaceae bacterium using experimental design. International Biodeterioration and Biodegradation. 86: 218-224. https://doi.org/10.1016/j.ibiod.2013.09.022

[11] Ouachtak, H., El Haouti, R., El Guerdaoui, A., Haounati, R., Amaterz, E., Addi, A.A., Akbal, F. and Taha, M.L., 2020. Experimental and molecular dynamics simulation study on the adsorption of Rhodamine B dye on magnetic montmorillonite composite γ-Fe2O3@ Mt. Journal of Molecular Liquids, 309, p.113142. https://doi.org/10.1016/j.molliq.2020.113142

[12] Alexander, J.A., Ahmad Zaini, M.A., Surajudeen, A., Aliyu, E.N.U. and Omeiza, A.U., 2019. Surface modification of low-cost bentonite adsorbents—A review. Particulate Science and Technology, 37(5), pp.538-549. https://doi.org/10.1080/02726351.2018.1438548

[13] Yuan, P., Fan, M., Yang, D., He, H., Liu, D., Yuan, A., Zhu, J. and Chen, T., 2009. Montmorillonite-supported magnetite nanoparticles for the removal of hexavalent chromium [Cr (VI)] from aqueous solutions. Journal of hazardous materials, 166(2-3), pp.821-829. https://doi.org/10.1016/j.jhazmat.2008.11.083

[14] Mockovčiaková, A., Orolínová, Z. and Škvarla, J., 2010. Enhancement of the bentonite sorption properties. Journal of Hazardous Materials, 180(1-3), pp.274-281. https://doi.org/10.1016/j.jhazmat.2010.04.027